AIP Advances

Polarization-based surface enhanced Raman scattering from single colloidal DNA decorated with 3 nm silicon nanoparticles

Cite as: AIP Advances **11**, 105206 (2021); https://doi.org/10.1063/5.0061671
Submitted: 28 June 2021 • Accepted: 10 September 2021 • Published Online: 04 October 2021

Kevin Mantey, Lucia Quagliano, Ayman Rezk, et al.

Polarization-based surface enhanced Raman scattering from single colloidal DNA decorated with 3 nm silicon nanoparticles

Cite as: AIP Advances 11, 105206 (2021); doi: 10.1063/5.0061671
Submitted: 28 June 2021 • Accepted: 10 September 2021 •
Published Online: 4 October 2021

Kevin Mantey,[1] Lucia Quagliano,[2] Ayman Rezk,[3] Simonetta Palleschi,[4] Laila Abuhassan,[5] Ammar Nayfeh,[3] Ersin Bahceci,[6] and Munir H. Nayfeh[1,a)]

AFFILIATIONS

[1] Department of Physics, University of Illinois at Urbana-Champaign, 1110 W. Green Street, Urbana, Illinois 61801, USA
[2] Institute of Materials for Electronics and Magnetism IMEM, Italian National Research Council, CNR, Parco Area delle Scienze 3/A, 43124 Parma, Italy
[3] Electrical Engineering and Computer Science, Khalifa University, Abu Dhabi 127788, United Arab Emirates
[4] Department of Environment and Health, Istituto Superiore di Sanità, Rome, Italy
[5] Department of Physics, University of Jordan, Amman, Jordan
[6] Department of Metallurgical and Materials Engineering, Iskenderun Technical University, 31200 Hatay, Turkey

[a)] **Author to whom correspondence should be addressed:** m-nayfeh@illinois.edu

ABSTRACT

Surface enhanced Raman scattering (SERS), in which sample molecules are placed in the proximity of conducting nanostructures, subjects the molecules to intense electron oscillation (plasmon) field. The intense field, however, may cause heavy distortion and thermal damage to the molecule as well as non-separable and heavy convolution with the metal electronic structure. We utilized 3-nm red luminescent Si nanoparticles decorating the DNA molecules (drawn electrostatically) to enhance Raman scattering in solution at 532 nm. We demonstrated that the nanoparticles enhance the spectral resolution and intensity of vibrations of DNA by two orders of magnitude and reveal vibrations that are otherwise weak or forbidden. Theoretically, we conducted calculations of Mie scattering and three-dimensional finite-difference time-domain scattering and obtained the wavelength dependence of the near-field distribution from single or dimer Si particles. The simulations show moderate intensity enhancement (25–40-fold) and exciton resonances. Moreover, it shows that the near field is highly confined, extending only to 3–5 Å from the Si particle (atomic scale) compared to several nanometers for metal nanoparticles. The observed SERS-type characteristics are understood in terms of polarization-based light scattering, which is possible by the use of Si of highly reduced size for which the polarizability and exciton processes are strong. However, multilayers contribute to metal SERS, and monolayers/single molecules dominate the Si case. Weaker but highly confined, ultra-short range polarization-based scattering provides an alternative to plasmon and Mie scattering, while providing practical, straightforward interpretation of vibration printing of bio-medical species without compromising the molecular structure.

I. INTRODUCTION

Surface enhanced Raman scattering (SERS),[1,2] in which sample molecules are placed within atomic distances from sharp nanoscale metal structures, increases scattering of external light (laser light, for example) by several orders of magnitude. This increases the sensitivity of vibration fingerprint recognition provided by the otherwise highly weak Raman spectroscopy. Several resonant processes are normally exhibited by the molecule-metal system, including metal plasmonic (in metal) Mie scattering and molecular and charge transfer (CT) between the metal and molecule processes. The enhanced scattering/sensitivity arises when the external light resonantly interacts with one or more of the natural resonances of the system simultaneously. The most dominant of the resonances is the plasmonic resonance, which is resonance excitation of oscillations of abundant "free" electrons in the conduction band of the nano-metal.[3]

Plasmonic resonance results in focusing the light of certain wavelengths (in the visible region for gold) to a small spatial nano-region (hotspot) within a few nanometers from the metal nano-structure.[4] A molecule residing in the hotspot is, therefore, subjected to a much stronger electric field than the incident field. With a quartic (fourth power E^4) dependence on the light field,[5,6] the Raman response becomes highly enhanced. Enhancement factors can be as high as many orders of magnitude, which are sufficient to allow even a single molecule to be detected.[6–8] Typical metals used are gold and silver as the plasmon resonance in those materials is within the visible range. Nano-structures can be free-standing or in the form of roughness on a metal surface. Preparation of nano-structures can be through electrochemical roughening, metallic coating of a nano-structured substrate, or deposition of metallic nanoparticles (often from a colloidal form).

The strong enhanced process, however, is not without major disadvantages. First, absorption and dissipation processes in metals can lead to release of heat (plasmonic heat) due to charge motion. This can alter or decompose the molecular sample, causing unwanted modifications.[9,10] Second, the electronic interaction of the metal surface with the molecule can cause extreme distortion and damage due to the large polarizability of the conducting electron states in the metal. Charge transfer from the Fermi level of the metal to the molecular levels (and from the molecular levels to the Fermi level) and the rise of a strong dipole–dipole deformation potential effectively take the two into a single system with coupled, non-separable electronic resonances. In general, the system can be represented or modeled by a number of resonances including metal plasmon resonance at ω_P, molecular resonances or energy levels at ω_{mol}, and charge-transfer resonances at ω_{CT}, with some underlying quantum effects. Strong quantum mixing between allowed and forbidden transitions modifies not only the optical selection rules but also the relative intensities of spectra, which may diminish some and allow others. As a result, the measured characteristics may not be exactly the characteristic of the original isolated molecule, requiring heavy de-convolution, hence hindering straightforward interpretation. In fact, the strong enhancement stems from the fact that the molecule and the metal become closely coupled (dominated by those at the Fermi level although all of the metal levels are involved). Finally, single molecule detection suffers from fluctuations and lack of reproducibility as intensity enhancement of $\sim 10^7$–10^8 and atomic- or molecular-scale focusing may not be realized as reliable enough in plasmonic hot spots using a spherical, triangular, rod-like, or nano-star metal geometry.[11]

Non-plasmonic or plasmon-free material, such as nano-structured dielectrics and semiconductors, has been proposed as an alternative material to metals[12–23] to alleviate strong electronic coupling, nonlinear structural deformations, and thermal damage. Studies using semiconductor nanoparticles showed enhancement in the Raman signal of adsorbed molecules[24,25] considerably lower than that for metals, which was attributed to the inaccessibility of the plasmon resonance. Although it is hoped that quantum confinement induced bandgap edges might play the role of metallic Fermi levels in those systems, it is not clear if one can find an appropriate material that provides such features. Moreover, it is not clear how to maximize or magnify the enhancement factor by tailoring the semiconductor so that several possible resonances in the system coincide at a single laser line in the visible region. For instance, there is ambiguity in the ability to access the size scale of individual particles or configurations of nanoparticles (dimers, clusters, or arrays) that allow quantum confinement control of exciton resonances and Mie scattering resonance simultaneously since such a condition would require conflicting size conditions. Doping of semiconductors may be used to increase the electron density in the conduction band. However, for plasmonic resonances to occur in the visible or near infrared portion of the spectrum, it would require extremely heavy doping, especially in the cases of silicon, germanium, and III–V semiconductors. Very high doping may, however, pose challenging solubility problems,[13] and high conductivity may hinder electrochemical processes that are used for the dispersion of bulk wafers into nanoparticles.[26–31]

In this paper, we conduct experimental and theoretical studies to examine the feasibility of using intrinsic ultra-small sub 3-nm luminescent silicon nano-structures/nano-particles instead of metal particles as an enhancer in Raman scattering measurements under wet solution conditions. These nanoparticles are interesting because they are high K materials (high refractive index). In high K dielectric materials, the induced polarization charge σ_p at the dielectric–vacuum surface interface is significant compared to the induced charge in a conductor plasmonic material–vacuum interface σ [$\sigma_p = \sigma$ (K − 1)/K], which for high K (13.32 for silicon) can be significant (=0.925 σ).

Specifically, silicon nanoparticles are useful for Raman studies for several reasons.[30,31] Quantum theory calculations using time dependent density functional theory (TDDFT) show that ultra-small silicon absorption in the visible region is small compared to that of bulk. Having a very small absorption and imaginary part results in little heating loss. Moreover, as they are dispersed from crystals with $\sim 10^{15}$/cc boron doping, they are essentially intrinsic (1 in a million would have boron), eliminating doping-induced conductivity and heating loss. In addition, DNA molecules under investigation will not be dominated by the particles because of their ultra-small size and radius of curvature. Moreover, because of their ultrasmall size, they will not exhibit plasmonic and Mie resonances in the visible region, preventing damage at the wavelength of operation. As to toxicity issues, they are considered to be the least toxic material and can dissolve in body fluid, flushing more easily than heavy metal nanoparticles. In addition, they are hydrophobic in aqueous media, allowing hydrophobic forces to form closely packed particle clusters or crystals, some of which would nucleate on the DNA molecules. This provides inter-particle gaps with atomic scale (3–10 Å), which provides additional field enhancement. Finally, they are luminescent, and as such, they may be used as an additional imaging tool when excited in the UV region.

We use incubation to decorate DNA molecules from the calf thymus in a colloid of silicon nanoparticles. The Raman spectra in the visible region are recorded with and without incubation to compare the intensities and spectral resolution and determine the degree of enhancement with wavelength. Theoretically, we use a three-dimensional finite-difference time-domain (3D-FDTD)[32,33] simulation to calculate the wavelength dependence of near-field electric field distribution from a single or dimers of 3-nm intrinsic Si nanoparticles with detailed input of wavelength dependence of the dielectric constant (derived from absorption or reflectivity measurements). In addition, we conduct Mie scattering calculations for a single and cluster of nanoparticles and map out the resonance frequencies with the size of the cluster over the range from vacuum UV

to infrared. We demonstrated that the nanoparticles significantly increase the resolution and intensity of Raman scattering from calf thymus DNA by two orders of magnitude. The calculations suggest that despite the reduced conductivity, the reduced size of the nanoparticles increases their polarizability to a level sufficient to enhance the near field scattering. Moreover, the reduced conductivity and reduced size shift plasmon and Mie resonance scattering out of the visible range, hence, alleviates strong couplings, distortions, and thermal damage, as well as non-separability and heavy-convolution of the electronic structures of the molecule and the silicon nanoparticle. The luminescent nano-silicon exhibits some aspects of surface enhanced Raman scattering (SERS)-type characteristics while providing practicality and straightforward interpretation of vibration fingerprinting of sensitive bio-medical and chemical species without compromising the luminescence.

II. EXPERIMENTAL MEASUREMENTS

The synthesis of nanoparticles was described elsewhere in detail.[26–31] In brief, a current-driven electrochemical reaction in a lateral configuration is used. Strips of a p-type (4–8 **Ω** cm boron doped) ⟨100⟩ oriented silicon wafer are placed vertically in a hydrogen peroxide H_2O_2/HF etchant mixture bath. A current source is attached to the positive electrode on the wafer and the negative electrode on a platinum wire in the solution. The current drives the etching reaction on the wafer. A larger current density increases the etching rate and causes smaller structures to form. Alternatively, the same starting silicon wafer is dipped in hexachloro-platinic acid for a certain period of time, which plates the wafer with platinum, which prefers to clump into small droplets. The sample is removed from the plating bath followed by dipping in the H_2O_2/HF etchant. The peroxide dissociates on the platinum spheres, oxidizing the surrounding silicon, which is removed by the HF. This effectively allows the platinum droplets to "bore" into the silicon surface. The rapid oxidation and removal produce a silicon nanoparticle-covered surface. We then rinse and sonicate the treated wafer in a solvent of choice, which forms a suspension of H-terminated silicon (Si–H) nanoparticles. This catalyst method cannot achieve the smaller scale structures obtainable with the driven current method but produces a much larger yield.

A pre-prepared commercial DNA colloid is mixed with and incubated in the nanoparticle colloid. Particles get drawn by electrostatic forces and bind on the DNA. In the process, DNA gets coated as schematically depicted in Fig. 1(a). The coating of DNA is expected not to be uniform, but it is comprehensive. Due to the hydrophobicity of the Si–H system in an aqueous environment, we expect some clustering and aggregation with a size from several nanometers to a 100 nm. This is a model configuration that represent closely packed H-terminated particles with each having a Si–H monolayer termination of 1-Å thickness. Such particles in an aqueous environment are driven by hydrophobic forces as shown in Figs. 1(b) and 1(c).[28] Hydrophobic forces can make colloidal crystals with closely packed particles, some of which would nucleate on the DNA molecules. This provides inter-particle gaps on atomic scale, 3–10 Å.[27,28] The Raman setup used is depicted in Fig. 2. The second harmonic of a Nd:YAG laser with an output at a wavelength of 532 nm is first sent through an aperture and then a monochrometer to clean the laser line. It is then focused on the liquid sample, and

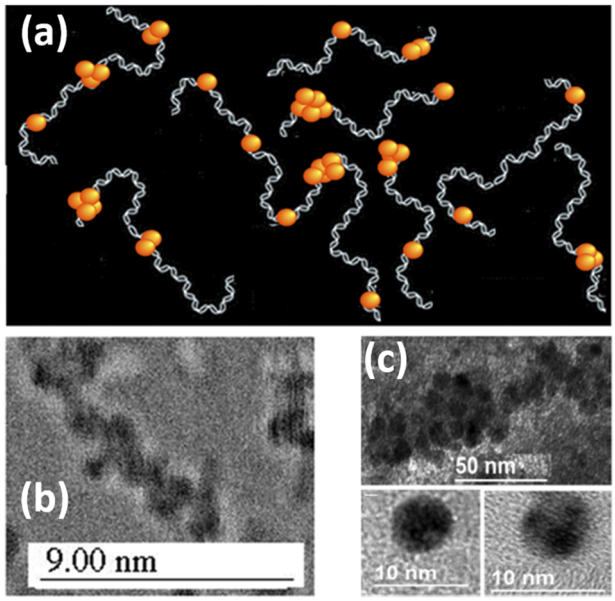

FIG. 1. (a) Cartoon of DNA molecules with a variety of multi-particle closely packed clusters of silicon nanoparticles decorating the molecules. (b) TEM image of 1-nm particles with close packing gaps resulting from hydrophobic forces on surfaces. Reproduced from Belomoin *et al.*, Appl. Phys. Lett. **80**, 841 (2002), with the permission of AIP Publishing. (c) TEM image of 3-nm particles with close packing gaps resulting from hydrophobic forces. Reproduced with permission from Enders *et al.*, AIP Adv. **9**, 095039 (2019). Copyright 2019 Author(s), licensed under a Creative Commons Attribution 4.0 License.

the scattering is collected by a lens assembly, which focuses the light on a pinhole to the monochrometer. The light then goes through yet one more monochrometer before falling on a liquid nitrogen cooled CCD, which collects the spectrum.

We now present some spectral scattering measurements, as shown in Fig. 3. The figure gives the results for the solvent alone, DNA on solvent without the nanoparticles, and the DNA decorated with the nanoparticles in the solvent. We first note that the sharp spikes are due to cosmic rays. As the scattering from a liquid sample is small, relatively long integration times (800 s) were

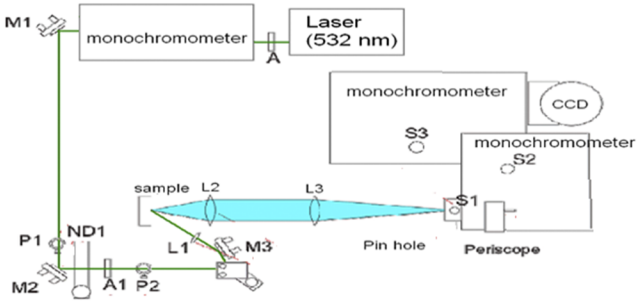

FIG. 2. Raman experimental setup. The second harmonic of a Nd:YAG laser at a wavelength of 532 nm is used, and a liquid nitrogen cooled CCD collects the scattering spectrum.

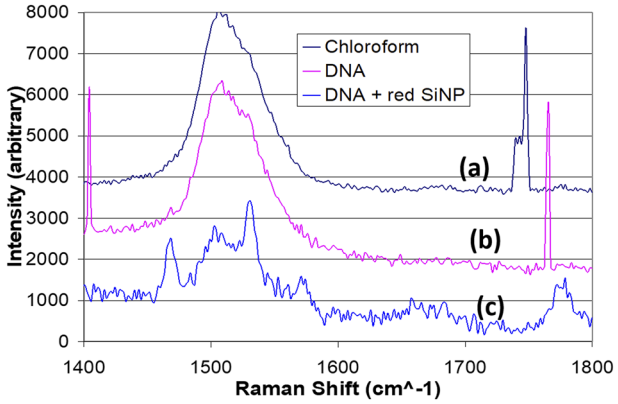

FIG. 3. SERS Raman scattering intensity as a function of the shift over the range 1400–1800 nm. (a) DNA in a chloroform solution decorated by silicon nanoparticles. (b) DNA in chloroform without the nanoparticles. (c) Chloroform liquid sample. It shows enhancement of DNA Raman scattering in the presence of silicon nanoparticles.

necessary. During this time, cosmic rays can strike the detector, leaving a buildup of charge. This is what causes the sharp spikes in the raw spectra and can be ignored. Second, three new peaks appear in the DNA sample + SiNP in the region from 1450 to 1600 cm^{-1} that could not be readily seen with the DNA (while they are not shown here, they were not visible with the SiNP alone either). These match with three peaks found with the silver SERS corresponding to vibrations in the backbone (at 1468 cm^{-1}) and base pairs (at 1530, 1574 cm^{-1}). There appears to be a shoulder in the DNA data near 1530 cm^{-1}. If we take that to be a Raman peak, then the enhancement with the silicon nanoparticles is only on the order of 100, which is less than that with silver nanoparticles.

Despite being weaker than metal enhancement, the Raman scattering from DNA molecules decorated by the silicon nanoparticles is strongly enhanced relative to the same molecules in solution. The estimated enhancement factor of the order of 10^2 is still a large surface effect. This represents an enormously enhanced Raman cross section compared to the intensity expected from the same number of non-decorated molecules. This suggests that the Raman signals measured originate from decorated DNA molecules and we are able to observe them because they are enhanced through the SERS effect. However, the existence of any enhancement is still an interesting result whose fundamental mechanism needs elucidation. For instance, the particles may interact with ions in the solution, interact with chemical groups on the DNA itself to provide a charge resonant structure, or strongly scatter the incident light into hot spots.

III. THEORETICAL

A. Semiconductor vs metal: Bandgap edge vs Fermi level

The process is discussed with the help of the restricted energy level diagram shown in Fig. 4. It shows the ground state (HOMO), the first excited state (LUMO), and the second excited state of the sample molecule. It also shows the top edge of the valence band of the particle as well as the bottom edge of the several bandgaps with their associated bandgaps. Those include the direct, quantum confinement, indirect, and the optical (emission) bandgaps at 3.2, 2.3, 1.1, and 2 eV, respectively.[30,31] It also shows the dominant transitions. First, the charge transfer (CT) from the ground state of the molecule to the conduction band of the particle as well as the transfer from the valence band of the particle to the first excited state of the molecule is observed. These represent the interaction between the two systems and are labeled by their transition dipole moment μ_{CT}. The dipole moments of the exciton (ex) transitions between the states of the nanoparticles are labeled μ_{ex}, while those between the molecular states (molecular processes) are labeled μ_{mol}. The rate of the Raman scattering $R_{ex\text{-}CT}(\omega)$, which is dominated by exciton (ex) transitions and charge exchange (CT) transitions, as a function of frequency ω of the external field can be written as[34]

$$R_{ex-CT}(\omega) = \frac{(\mu_{ex}\cdot E)(\mu_{CT}\cdot E)h_{ex-CT}\langle i|Q_k|f\rangle}{((\omega_{Mic}{}^2-\omega^2)+\gamma_{Mic}{}^2)((\omega_{Mic}{}^2-\omega^2)+\gamma_{CT}{}^2)((\omega_{ex}{}^2-\omega^2)+\gamma_{ex}{}^2)}, \quad (1)$$

where ω_{Mie}, ω_{CT}, and ω_{ex} are the resonance frequencies corresponding to the Mie scattering off of the nanoparticles, the frequency for charge exchange processes between the molecule and the nanoparticle, and the frequency for exciton excitation in the nanoparticle, respectively. Those frequencies are not necessarily equal or close to each other and can be very different from each other. The gammas γ_{Mie}, γ_{CT}, and γ_{ex} are the corresponding damping rates. E is the amplitude of the near field, μ_{CT} and μ_{ex} are the transition dipole moments defined above, $h_{ex\text{-}CT}$ is the Herzberg–Teller coupling constant (coefficient), and $\langle iQ_kf\rangle$ is the optical transition between the initial and final state. Note the denominator is the product of the resonance terms. The numerator contains the coupling of the three resonances. The requirement that the numerator of this expression should not vanish results in selection rules.

For a metallic nanoparticle, whose plasmon resonances are out of the visible range, it is not necessary to show the plasmon resonance factor. Moreover, there are no band edges available for charge transfer. These are replaced by the Fermi level. Furthermore, enhancement stemming from exciton (or interband) transitions involving the creation of an electron–hole pair is absent, but alternative enhancement may be derived from molecular resonances (transitions). Thus, one can write for such a metal a theoretical expression similar to that of the silicon nanoparticles given above, with the band edges replaced by the Fermi level and the exciton resonance replaced by the molecular resonance. We obtain the following expression (https://pubs.rsc.org/image/article/2017/fd/c7fd00138j/c7fd00138j-t5_hi-res.gif):[34]

$$R_{mol-CT}(\omega) = \frac{(\mu_{mol} \cdot E)(\mu_{CT} \cdot E)h_{mol-CT}\langle i|Q_k|f\rangle}{((\omega_{Mic}{}^2 - \omega^2) + \gamma_{Mic}{}^2)((\omega_{CT}{}^2 - \omega^2) + \gamma_{CT}{}^2)((\omega_{mol}{}^2 - \omega^2) + \gamma_{mol}{}^2)}. \quad (2)$$

Finally for a certain metal, if a plasmon resonance is strong and its frequency is near the visible range, then an expression may be written for this case where the plasmon resonance is introduced explicitly as shown in the following expression:[34]

$$R_{mol-CT}(\omega) = \frac{\left(\mu^{\alpha}{}_{mol} \cdot E_{sp,\alpha}\right)\left(\mu^{\beta}{}_{CT} \cdot E_{sp,\beta}\right)h_{mol-CT}\langle i|Q_k|f\rangle}{\left((\varepsilon_1(\omega) + 2\varepsilon_0)^2 + x\varepsilon_2{}^2\right)((\omega_{CT}{}^2 - \omega^2) + \gamma_{CT}{}^2)((\omega_{mol}{}^2 - \omega^2) + \gamma_{mol}{}^2)}, \quad (3)$$

where in this expression, the first resonance is the surface-plasmon resonance at $\varepsilon_1(\omega) = -2\varepsilon_0$, where ε_1 is the real part of the dielectric constant of the metal and ε_0 is the dielectric constant of the surrounding medium, and ε_2 is the imaginary part of the metal dielectric constant. The resonance lies entirely within the metal nanoparticle. The term χ is a geometrical-based constant factor that accounts for the deviation of the nanoparticle from a spherical shape. The second and the third resonances represent charge-transfer and the molecular resonances, respectively.

In general, quantum effects play a role as discussed above; however, we will only consider classical optical properties in the present work. It is not always clear, however, in the case of small particle sizes if their optical constants must be corrected to account for quantum effects. The silicon nanoparticle is unique since its direct band edge (3.3 eV) is in the UV region, as well as the plasmon and the Mie resonances, and the nanoparticle-DNA molecule coupling is out of reach. The quantum confinement bandgap of silicon at a size of 3-nm diameter, however, is at 2.3 eV. This is near the operating photon energy of 2.33. However, this transition is much weaker than the transition at the direct bandgap at 3.3 eV.[30,31] Assuming quantum resonance effects are not strongly in play, we only use a classical electromagnetic (EM) treatment. The calculations as such may not fully describe the actual system.

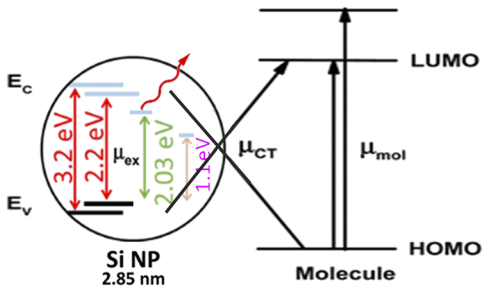

FIG. 4. Restricted energy level diagram of the process. It shows the ground state (HOMO), the first excited state (LUMO), and the second excited state of the molecule. It also shows the top edge of the valence band of the particle as well as the bottom edge of the several conduction bands: the direct, quantum confinement, indirect, and the optical (emission) bandgaps are at 3.2, 2.3, 1.1, and 2 eV, respectively. The figure also shows the dominant transitions.

B. Maxwell's solution of field distribution/ enhancement by silicon nanoparticles

The Finite-Difference Time-Domain (FDTD) method is a discrete solution to Maxwell's equations based on central difference approximations of the spatial and temporal derivatives of the curl-equations.[32] A perfectly matched layer (PML) makes the FDTD method capable of simulating unbounded problems. Moreover, the procedure is capable of absorbing evanescent waves and near fields. Another feature, which was made possible by using the basic Yee algorithm, allows the procedure to handle modeling of very complex geometries.[33] This is augmented with the use of sub-cell modeling techniques and local sub-grids, that is, a sub-grid is embedded within the global grid in order to locally resolve fine geometric structure without sacrificing the global space/time scale. The application of sub-cell models and sub-gridding methods enhances the efficiency and the accuracy of the FDTD method for modeling very complex systems.

Next, we apply the FDTD method to 3-nm Si particles to determine the distribution of the scattering near the field as a function of the incident wavelength. We map out the response in the region 350–1600 nm (3.54–0.775 eV). The range includes the relevant bandgaps for the Si nanoparticle, including the direct, quantum confinement, and indirect bandgaps at 3.2, 2.3, and 1.1 eV, respectively. The quantum confinement bandgap at 2.3 eV is acquired by silicon with a size of 3-nm diameter. Moreover, silicon with a size of 3 nm exhibits an optical bandgap at 2 eV due to luminescence over the range 550–750 nm. We first focus on a free-standing

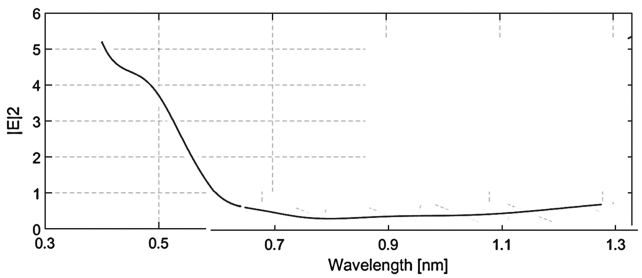

FIG. 5. $E^2/E_0{}^2$ normalized to the incident intensity as a function of wavelength over the range 300–1400 nm for a free-standing 3-nm Si particle. It shows that the response is mainly enhanced in the UV and visible regions.

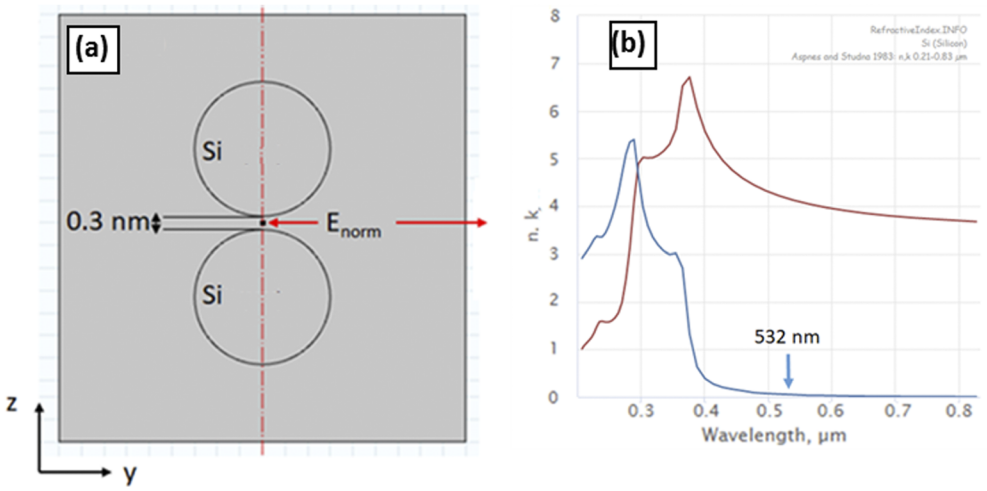

FIG. 6. (a) Model for calculation of field distribution of a multi-particle configuration of two close-packed 3-nm diameter particles with a gap of 0.3 nm. (b) The inputted refractive index n and the absorption length k as a function wavelength.

3-nm Si particle. Figure 5 shows the scattered field normalized intensity to the incident intensity (E^2/E_0^2) as a function of wavelength over the range 300–1400 nm. It shows that the response is mainly enhanced in the UV and visible regions. The enhancement reaches a factor of 8–10 at short wavelength above the edge of the direct bandgap at 3.25 eV. As the wavelength increases, the enhancement drops, exhibiting a peak or some flattening at a level of a factor of 5, and then continues to drop through the quantum mechanical confinement bandgap at 2.3 eV (540 nm). Below this bandgap, the response continues to fall, passing through the opening of the optical gap (2.1 eV) and the luminescence band over the range 2.25–1.65 eV (550–750 nm),[26–31] resulting in near quenching of the external field. It is to be noted that over the particle's luminescence band, fast electron hole pair recombination takes place. Beyond the luminescence region, the response stays nearly flat at a small fraction of the incident intensity before it shows an enhancement threshold commencing at the opening of the indirect bandgap at 1.1 eV.

We now calculate the near-field enhancement by multi-particle architectures. We calculated the near field distribution of two close-packed 3-nm silicon nanoparticles with a gap or open bridge of 3 Å (dimer) in a configuration as shown in Fig. 6(a). This is a model configuration to illustrate and display some characteristics. As mentioned above, it represents closely packed H-terminated particles with each having a Si–H monolayer termination of 1-Å bond length. The particles are driven by hydrophobic forces to form colloidal crystals as is shown in Figs. 1(b) and 1(c).[27,28] The inputs refractive index n and the absorption length k as a function wavelength are shown in Fig. 6(b).

In Figs. 7(a)–7(c), a 2-D cut of the near-field distribution is displayed in 2-D using the color code shown on the right of each figure. We show the contours of the intensity of the scattered electric field normalized to those of the incident field strength at three different wavelengths (400, 600, and 1500 nm). Those numerical results on the electric field strength distribution showed enhancement near the particles. It strongly drops with distance from the surface of the particle, and as such, it is called surface field, or near field. This enhancement does not originate from or is not assigned to excitation of plasmons. One should note again that the enhancement is associated just with the sharp points and a sharp change in the dielectric constant at very small distances. The particles represent wedges or sharp dielectric points.[35] In fact, this kind of fields has been known from radio-physics and electrodynamics of semiconductors and dielectrics, not metal, with the nature associated just with the irregular character of the surface and the strong decrease with distance from the surface. The nanoparticle here represents an element of surface roughness. Figure 7(d) shows the schematic of the field lines for two particles. The field lines are similar to two collinear dipoles pointing in the same direction. The dipoles are induced by the external field, yet they are strongly interacting. The effect is a pure electrodynamical effect, associated with a very strong change in the electric field near the top of the nanoparticles, when one moves away from the surface. These sharp points or nanoparticles are named as active sites or hot spots. The electric field and its derivatives differ so strongly in space.

Figure 8 plots the detailed intensity of the scattered electric field between the two particles normalized to the intensity of the incident electric field as a function of the wavelength of the electric field of the incident light. The response shows that the intensity of the near electric and hence the SERS spectrum can vary considerably with excitation wavelength. First, it shows that the intensity enhancement in the region between the particles takes place in the infrared region, making the effect significant across the full range of the UV–visible–infrared part of the spectrum.

Since Fig. 7 shows that there was no hotspot in the infrared region for a single nanoparticle, the emergence of a hotspot in the infrared for a doublet of particles can be assigned to the strong interaction between the particles. Second, in the visible region, it

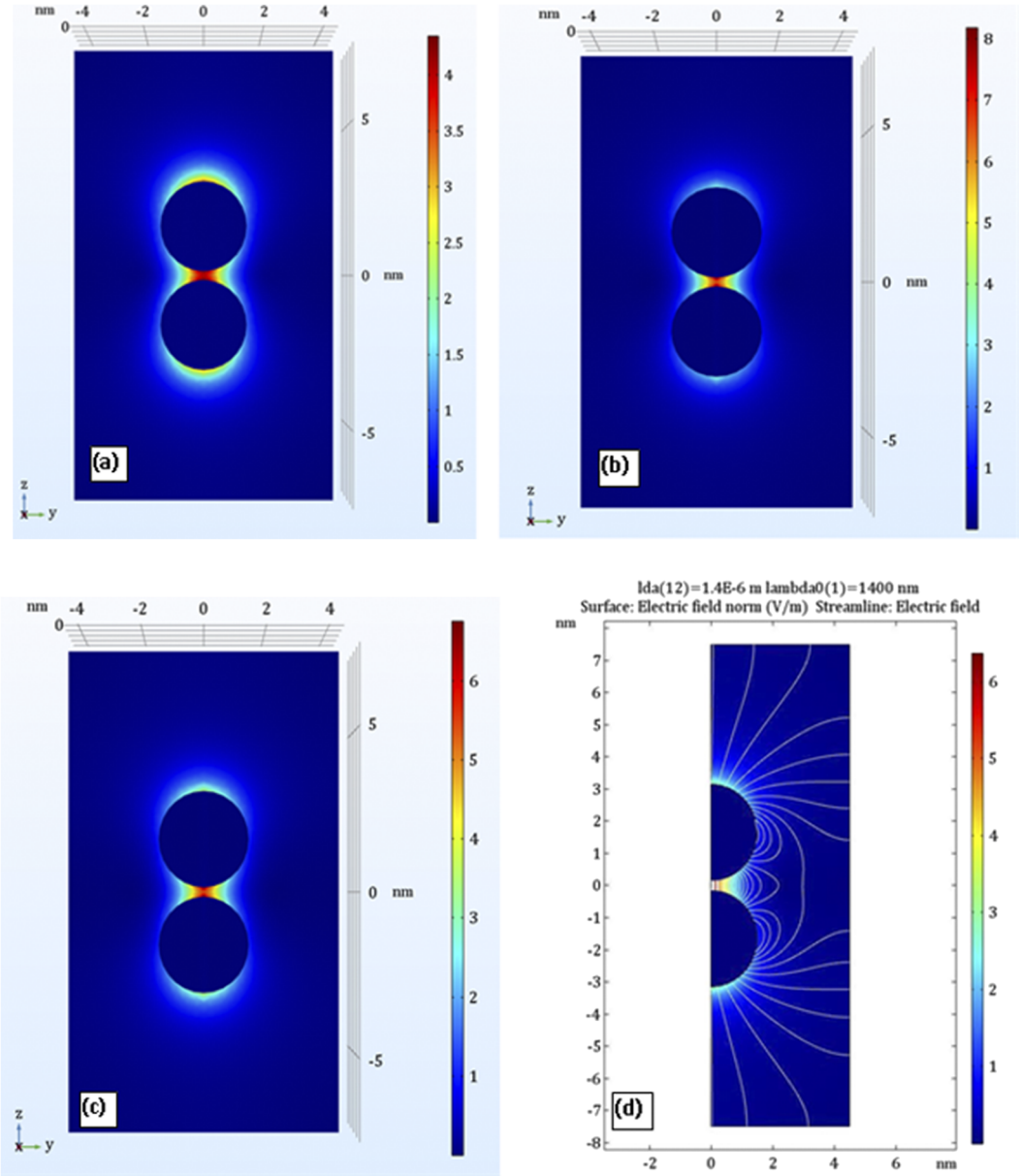

FIG. 7. x-z cross section contours of the near field intensity of scattered electric field normalized to the incident field strength E2 with the color code shown on the right for three wavelengths: (a) 600, (b) 400, and (c) 1400 nm. In those figures, a 2-D cut of the near-field distribution (d) shows schematic of the field lines for one of the (c) cases. The field lines are similar to two collinear dipoles pointing in the same direction.

shows a smooth wavelength with some resonance structure riding on it, with some good visibility (max − min)/(max + mim) ~ 0.053 (a pure resonance case has a visibility of 2). The flat or DC underlying enhancement may be due a classical geometrical effect. This enhancement does not originate from or is not assigned to excitation of plasmons. One should note again that the enhancement is associated just with the sharp points (nanoparticles) and a sharp change in the dielectric constant at very small distances. For excitation in the deep infrared region below the indirect bandgap, the response approaches a smooth flat electric field intensity enhancement at a level of 5. This may be attributed to a dipole–dipole interaction between the two particles. In addition, the response shows onsets of local enhancement peaks due to the quantum molecular structure of the material at ~1100, 560, and 375 nm. In addition, it shows a

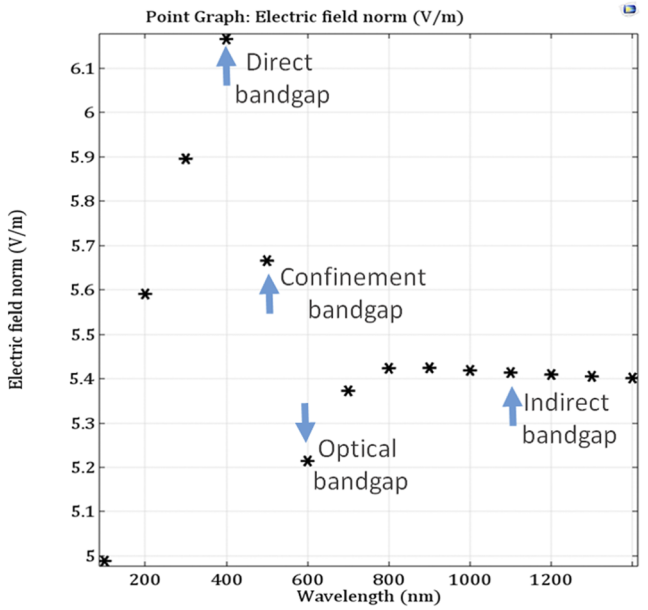

FIG. 8. Plot the scattered electric field between the two particles normalized to the electric field of the incident light as a function of the wavelength of the incident field.

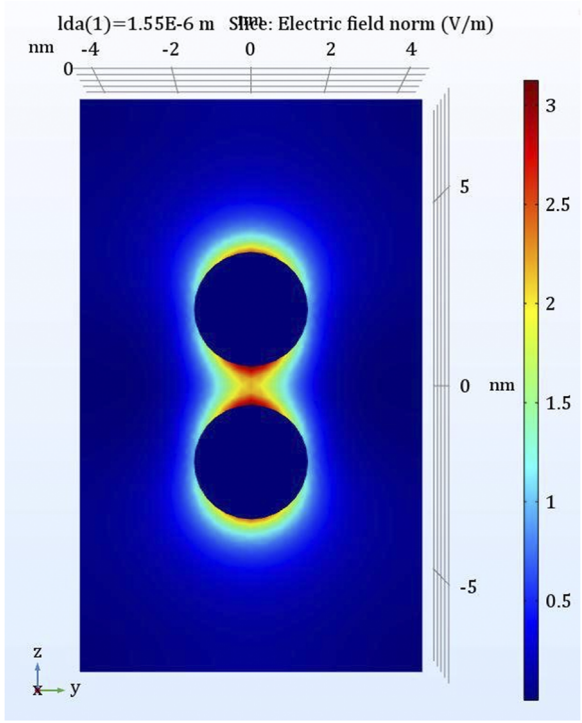

FIG. 9. 2-D cut of the near-field distribution is displayed in 2-D using the color code shown on the right for two particles with a gap of 1 nm.

sharp drop in the response in the visible region with a maximum dip at ~600 nm. Those peaks lie at the openings of the indirect bandgap at 1.1 eV, confinement bandgap at 2.3, and direct bandgap at 3.3 eV results. However, at the opening of the optical bandgap where the system undergoes luminescence, i.e., at 600 nm (2 eV), we see a dip or reduction. This phenomenon may reflect the fact that at this energy, there is strong and fast electron–hole charge recombination that produces red light, which reduces the polarization of the particle and inhibits the acceleration of the e-h charges in the particle. The flat underlying response reflects the geometrical response based on the curvature or size of the nano-structures. The sharp peaked structures represent the density of states at the opening of the bandgap. Figure 9 shows the calculation for a case where the gap between the nanoparticle is increased from 0.3 to 1 nm (size of a DNA molecule) to examine the range of interaction between the particles. It shows the intensity drops to 65% over a distance of 3.5 A from the surface of the nanoparticle. Thus, the field is highly focused. The range of the hotspot reaches out to 7–10 Å from the surface of either one, sufficient for a DNA strand to fit between the nanoparticles. Moreover, Raman scattering is highly nonlinear, depending on E^4, which makes the "effective" focal spot even tighter, and the spatial resolution may be set at ~5 Å. Since the field dies out very sharply with the distance from the surface and since the scattering process is highly nonlinear, the field can hardly affect more than single-molecule thick layers. This makes the process highly selective spatially (atomic-scale or angstrom characteristics), a highly useful feature that alleviates damage of healthy tissue in biological applications.

It is to be noted that near field enhancement has been achieved in the neighborhood of two Si particles (dimers of spheres) as well as nano-disks as shown by Albella *et al.*[36,37] It corresponds to a dimer of silicon subwavelength spheres placed in close proximity. The size of each sphere is 150 nm in radius to keep their resonances in the near-infrared range of the spectrum. The gap was varied, with the smallest being 4 nm. Similar effects were observed when the spheres were made of GaP.[38]

C. Mie and plasmon resonance activities

In this section, we conducted Mie scattering[39–41] studies to evaluate their importance and contribution for larger clusters of nanoparticles. We applied them to individual silicon nanoparticles as well as to packed clusters of the particles. The theory involves direct analytical solution of Maxwell's equations of particles in the presence of an electromagnetic field E and B using series expansions of the involved fields and partial waves of different spherical symmetries to model the interaction of metallic or semiconductor nanoparticles with electromagnetic radiation. We use this study for a semi-analytical/numerical solution.[39–41] Figures 10(a) and 10(b) shows the extinction (sum of absorption and scattering) cross section for a cluster of sizes 1.5 and 5 nm (3 and 10 nm in diameter) corresponding to a single and ~9 nanoparticles as a function of wavelength in the range 250–800 nm. Figures 11(a) and 11(b) show parallel results for cluster sizes of radii of 25 and 40 nm (50 and 80 nm in diameter) corresponding to 1125 and ~4608 closely packed nanoparticles. The cluster of a size of 80 nm shows a resonance at 350 nm. For less than 50 nm, the resonances are in the deep UV region below 250 with a small cross section. For a cluster of 80 nm, we find Mie-type resonances in the UV region at ~300 with a cross section of

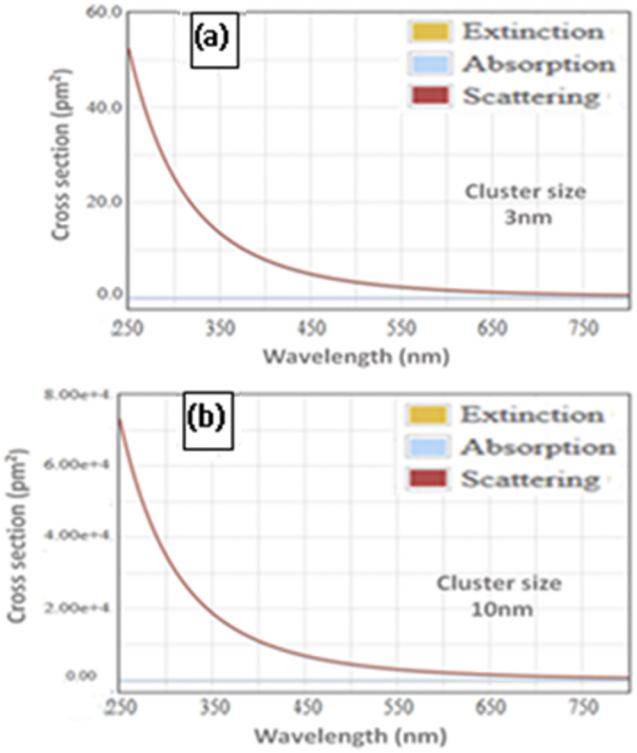

FIG. 10. Calculated Mie scattering cross section of single and close-packed clusters of Si nanoparticles. The cross section is plotted as a function of wavelength in the range 250–800 nm for clusters of a diameter of (a) 3 and (b) 10 nm.

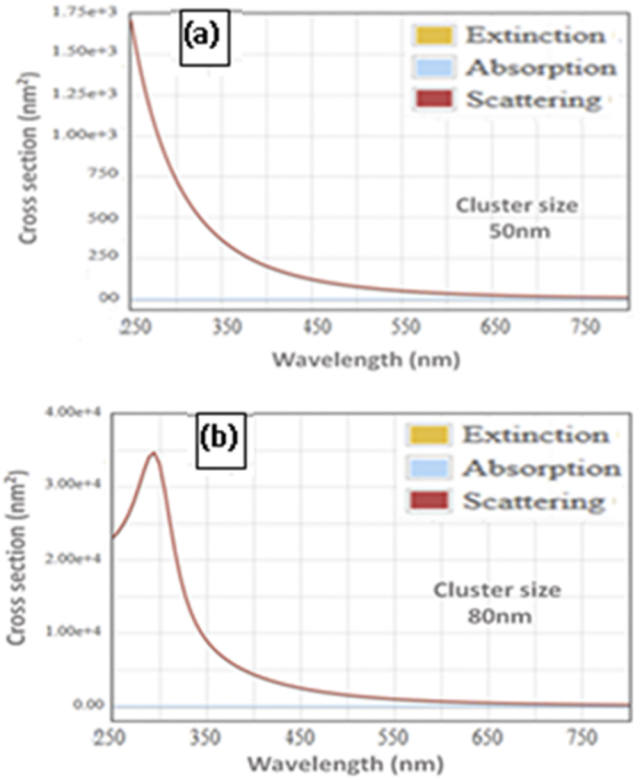

FIG. 11. Calculated Mie scattering cross section of single and close-packed clusters of Si nanoparticles. The cross section is plotted as a function of wavelength in the range 250–800 nm for clusters of a diameter of (a) 50 and (b) 80 nm.

3.5×10^4 nm^2 (3.5×10^{-14} m^2 or 3.5×10^{-10} cm^2), which is more than sevenfold the geometrical cross section (5×10^{-15} m^2).

In the studies shown in Figs. 10 and 11, we neglected the imaginary part of the refractive index. For bulk, the optical constants of silicon given in Fig. 6(b) show a residual imaginary component in the green area of ~0.03 magnitude, which is only 0.0056 of its maximum at 275. Figures 12(a) and 12(b) show a full quantum mechanical calculation of the absorption of the 1-nm particle. It was executed using many body theory of the time dependent density functional theory (TDDFT).[42] It shows very weak absorption in the visible region compared to the maximum, which shifts deeper to the UV region to 145 nm. In fact, the absorption picks up only for $\lambda < 470$ nm. In fact, at $\lambda = 468$ nm, it is 3.6×10^{-6} of the maximum. It is to be noted that the interaction may begin to show some sizably residual effect for particles of 150 nm radius (300 nm diameter) when the size is a good fraction of the wavelength (kr ~ 1).

As to the role of plasmon resonances, we can estimate the location of the plasmon resonance (ω_p) by considering the following formula, which defines the plasmon frequency:[43]

$$\omega_p = \left(\frac{4\pi N e^2}{\varepsilon_\infty m^*}\right)^{1/2}, \tag{4}$$

where m^* is the effective electron mass and N is the electron density. Since N is expected to be small in silicon conduction bands and since the plasmon frequency is proportional to the square root of N, ω_p is expected to lie deep in the infrared region. If one electron is promoted to its conduction band in a 3-nm particle having a volume V = 14.1×10^{-21} cm^3, we expect the charge density to be 7×10^{19}/cm^3 in the particle. Using $m^* = 0.25$ m in silicon and one electron in the conduction band gives a plasmon resonance at ~8 μm, well beyond the visible region of interest. It is to be noted that the particles were dispersed from wafers that have been pre-doped at a level of 5×10^{15}/cm^3. Thus, only 1 out of 10^5 particles would have a charge dopant. It is, however, plausible that a dynamic plasmonic process may take place. Due to surface reconstruction in our synthesis protocol, H–Si–Si–H dimer like sites form on the nanoparticle surface, which act as intrinsic charge traps. Radiation with wavelength at 532 nm (2.3 eV) excites above the quantum confinement bandgap (2.2 eV), and electron–hole pairs (exciton) are produced in the particle. Moreover, since the exciton's Bohr diameter is larger than the particle size, correlation between the positive and negative charge is reduced, allowing the heavy hole to be trapped on the dimer like sites before electrons can because of their higher speed. Such delayed trapping may provide a partial free electronic charge in the bulk of the particle.

Plasmon resonances of electrons in the valence bands shift toward the visible region because the electron density in the valence band is very high. In silicon, the density is ~5×10^{22} cm^{-3} so

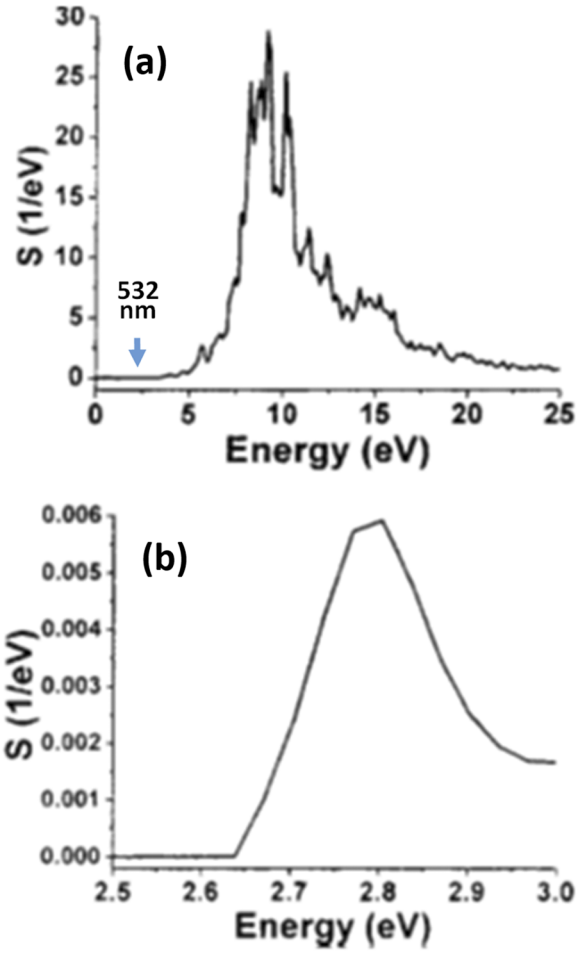

FIG. 12. (a) Full quantum mechanical calculation of the absorption of 1-nm silicon particle as a function of the photon energy using many body theory of the time dependent density functional theory (TDDFT). (b) A close up of the low energy portion of the full spectrum in (a). Reproduced with permission from Rao *et al.*, Phys. Rev. B **69**, 205319 (2004). Copyright 2004 The American Physical Society.

that plasmons emanating from the valence electrons tend to lie in the vacuum UV region (at ~275 nm). In comparison, for gold, $N = 5.9 \times 10^{22}/cm^3$ and $m^* = 1.09$ m, and the resonance occurs in the visible region at ~570 nm. Thus, any plasmon resonance effects in the Si particle would have little influence on the Raman enhancement in the visible region at 532 nm. Rather, it is expected to contribute a weak, wavelength independent (smooth) factor to SERS.

A plausible mechanism that may provide plasmonic charge is based on external surface doping, which may take place under the conditions of wet interaction in a colloid. For instance, if a charge complex is formed with an ion in the solvent and a fraction of charge is shared between the two, it is possible this can allow the particle to effectively have a partially free charge carrier. In fact, different adsorption mechanisms are possible depending on the environmental conditions. Studies using silver nanoparticles showed that at neutral pH, the SERS spectra are obviously much more enhanced than the SERS signals at acidic pH or at alkaline pH. The SERS signals after 16 h of interaction between the Ag colloid and the DNA solution were much better than the SERS just after the mixed liquid has been prepared. The results of the interaction of Ag sol molecules with nucleic acids were used to obtain the SERS spectra of DNA molecules. Furthermore, the process was used to study the adsorption behavior of solute bio macromolecules in different solvents.

Finally, the enhanced Raman scattering (SERS) in a mixture of DNA, and the Si nanoparticles confirm that the adsorption of the Si semiconductor quantum-dots/nanoparticles on the DNA molecules and that the nanoparticles are small enough, so they may not dominate the DNA molecule or cause modification or loss of functionality due to chemical attachment.

Metal nanoparticles, due to their abundant free charge carriers, can enhance the electromagnetic fields in their local vicinity in a Raman scattering experiment by a power of four.[20–23,44] SERS with silver nanoparticles coated with DNA in a solution has been demonstrated to increase the Raman scattering from calf thymus DNA by a factor of 10^5.[45] Little Raman enhancement has been noted in the literature near silicon based nanostructures on a solid porous silicon surface.[46] The enhancement was attributed to cavity resonances in the larger pores or particles (they had up to micrometer sized crystalline structure) or resonance with an excited state. In the present study, the particles used are much smaller (3-nm) in a liquid suspension.

IV. CONCLUSION

We utilized 3-nm silicon nanoparticles and their clusters in surface enhanced Raman scattering (SERS)-type measurements at 532 nm for DNA detection in solution without the use of a solid substrate. We demonstrated increases in the resolution and intensity of Raman scattering from calf thymus DNA by two orders of magnitudes while eliminating Mie and plasmonic resonance contributions, which cause heat damage as well as distortion to the molecular sample. The observed results are understood using three-dimensional finite-difference time-domain (3D-FDTD) simulations and polarization-based light focusing, which produces highly-confined, ultra-short range (angstrom-scale) hot spots. However, multilayers are responsible for the signal in metal-based SERS, and monolayers or single molecules dominate in the Si nanoparticle case, while providing straightforward interpretation of vibration of finger-printing of sensitive bio-medical and chemical species without heat damage and distortion of the molecular structure of the sample caused by excessive field strengths and enhancements resulting from Mie and plasmonic resonances. SERS is observed not only on rough surfaces but also on molecules adsorbed on colloidal particles of metals, dielectrics, and semiconductors, or on single nanoparticles. In particular, many works point out the appearance of strong enhancement or appearance of "active sites," or "hot spots," in the areas between very closely situated nanoparticles.

DATA AVAILABILITY

The data that support the findings of this study are available from the corresponding author upon reasonable request.

REFERENCES

[1] M. Fleischmann, P. J. Hendra, and A. J. McQuillan, Chem. Phys. Lett. **26**(2), 163 (1974).
[2] R. Signorini, C. Durante, L. Orian, M. Bhamidipati, and L. Fabris, Biosensors **9**, 57 (2019).
[3] D. Pines and D. Bohm, Phys. Rev. **85**(2), 338 (1952).
[4] M. H. Nayfeh, "Optics in nanotechnology," in *Optics in Our Time*, edited by M. Alamri, M. M. El Gomati, and M. S. Zubairy (Springer, 2016), pp. 223–264.
[5] E. J. Blackie, E. C. Le Ru, M. Meyer, and P. G. Etchegoin, J. Phys. Chem. C **111**(37), 13794 (2007).
[6] P. Alonso-Gonzalez *et al.*, Nat. Commun. **3**, 684 (2012).
[7] S. Nie and S. R. Emory, Science **275**(5303), 1102 (1997).
[8] E. C. Le Ru, M. Meyer, and P. G. Etchegoin, J. Phys. Chem. B **110**(4), 1944 (2006).
[9] M. Mahmoudi, S. E. Lohse, C. J. Murphy, A. Fathizadeh, A. Montazeri, and K. S. Suslick, "Variation of protein corona composition of gold nanoparticles following plasmonic heating," Nano Lett. **14**, 6 (2014).
[10] E. C. Le Ru and P. G. Etchegoin, *Principles of Surface-Enhanced Raman Spectroscopy: And Related Plasmonic Effects* (Elsevier, Amsterdam, The Netherlands, 2009).
[11] D. Radziuk and H. Moehwald, Phys. Chem. Chem. Phys. **17**, 21072 (2015).
[12] I. Alessandri and J. R. Lombardi, Chem. Rev. **116**, 14921 (2016).
[13] P. R. West, S. Ishii, G. V. Naik, N. K. Emani, V. M. Shalaev, and A. Boltasseva, Laser Photonics Rev. **4**, 795–808 (2010).
[14] G. V. Naik, V. M. Shalaev, and A. Boltasseva, Adv. Mater. **25**, 3264 (2013).
[15] G. Demirel, H. Usta, M. Yilmaz, M. Celik, H. A. Alidagi, and F. Buyukserin, J. Mater. Chem. C **6**, 5314 (2018).
[16] W. Ji, B. Zhao, and Y. Ozaki, J. Raman Spectrosc. **47**, 51 (2016).
[17] X. X. Han, W. Ji, B. Zhao, and Y. Ozaki, Nanoscale **9**, 4847 (2017).
[18] J. R. Lombardi and R. L. Birke, J. Phys. Chem. C **118**, 11120 (2014).
[19] H. Yamada, Y. Yamamoto, and A. Tani, Chem. Phys. Lett. **86**, 397–400 (1982).
[20] A. I. Barreda *et al.*, AIP Adv. **9**, 040701 (2019).
[21] A. B. Evlyukhin *et al.*, Phys. Rev. B **82**, 045404 (2010).
[22] R. Gómez-Medina *et al.*, J. Nanophotonics **5**, 053512 (2011).
[23] A. Etxarri *et al.*, Opt. Express **19**, 4815–4826 (2011).
[24] L. G. Quagliano, J. Am. Chem. Soc. **126**, 7393 (2004).
[25] I. Alessandri and J. R. Lombardi, Front Chem. **8**, 63 (2020).
[26] O. Ackakir, J. Therrien, G. Belomoin, N. Barry, J. Muller, E. Gratton, and M. Nayfeh, Appl. Phys. Lett. **76**, 1857 (2000).
[27] G. Belomoin, J. Therrien, A. Smith, S. Rao, R. Twesten, S. Chaieb, M. H. Nayfeh, L. Wagner, and L. Mitas, Appl. Phys. Lett. **80**, 841 (2002).
[28] B. Enders, A. Kocyigit, E. Bahceci, N. Elhalawany, A. Nayfeh, O. Alshammari, M. Alsalhi, and M. Nayfeh, AIP Adv. **9**, 095039 (2019).
[29] D. Nielsen, L. Abuhassan, M. Alchihabi, A. Al-Muhanna, J. Host, and M. H. Nayfeh, J. Appl. Phys. **101**, 114302 (2007).
[30] M. H. Nayfeh and L. Mitas, "Silicon nanoparticles: New photonic and electronic material at the transition between solid and molecule," in *Nanosilicon*, edited by V. Kumar (Elsevier, 2007), p. 1.
[31] M. H. Nayfeh, *Fundamentals and Applications of Nano Silicon in Plasmonics and Fullerenes: Current and Future Trends* (Elsevier Publishing, 2018).
[32] S. Tanev, J. Pond, P. Paddon, and V. V. Tuchin, *Advances in Optical Technologies/Biophotonics* (Hindawi Publishing Corporation, 2008), No. 727418.
[33] K. Yee, IEEE Trans. Antennas Propag. **14**(3), 302 (1966).
[34] J. R. Lombardi, Faraday Discuss. **205**, 105 (2017).
[35] V. P. Chelibanov and A. M. Polubotko, Opt. Spectrosc. **122**, 937 (2017).
[36] P. Albella, M. A. Poyli, M. K. Schmidt, S. A. Maier, F. Moreno, J. J. Sáenz, and J. Aizpurua, J. Phys. Chem. C **117**, 13573 (2013).
[37] M. Caldarola, P. Albella, E. Cortés, M. Rahmani, T. Roschuk, G. Grinblat, R. F. Oulton, A. V. Bragas, and S. A. Maier, Nat. Commun. **6**(18), 7915 (2015).
[38] P. Albella, R. Alcaraz de la Osa, F. Moreno, and S. A. Maier, ACS Photonics **1**, 524 (2014).
[39] G. Mie, Ann. Phys. **25**(3), 377 (1908).
[40] See https://nanocomposix.com/pages/tools for Nanocomposix, 2021.
[41] B. Guillaume, J. Phys. Chem. C **119**, 28586 (2015).
[42] S. Rao, J. Sutin, R. Clegg, E. Gratton, M. H. Nayfeh, S. Habbal, A. Tsolakidis, and R. M. Martin, Phys. Rev. B **69**, 205319 (2004).
[43] C. Kittel, A. Zettl, and P. McEuen, *Introduction to Solid State Physics* (John Wiley & Sons, New York, 2004).
[44] M. H. Nayfeh, "Optics in nanotechnology," in *Optics in Our Time*, edited by M. Alamri, M. M. El Gomati, and M. Suhail Zubairy (Springer, 2016), pp. 223–264.
[45] K. Weizhong, Z. Dianfeng, W. Jianzhong, and J. Kang, Appl. Spectrosc. **59**(4), 418 (2005).
[46] F. M. Liu, B. Ren, J. H. Wu, J. W. Yan, X. F. Xue, B. W. Mao, and Z. Q. Tian, Chem. Phys. Lett. **382**, 502 (2003).